Adsorbate-induced Modification of Surface Electronic Structure: Pyrocatechol Adsorption on the Anatase TiO_2 (101) and Rutile TiO_2 (110) Surfaces

Karen L. Syres[a‡], Andrew G. Thomas[a], Wendy R. Flavell[a], Ben F. Spencer[a], Federica Bondino[b], Marco Malvestuto[c], Alexei Preobrajenski[d], Michael Grätzel[e]

[a] School of Physics and Astronomy and Photon Science Institute, Alan Turing Building, The University of Manchester, Oxford Road, Manchester, M13 9PL, UK.

[b] IOM CNR, Laboratorio TASC, S.S. 14 Km. 163,5, I-34149 Basovizza, Trieste, Italy.

[c] Sincrotrone Trieste S.C.p.A. di interesse nazionale Strada Statale 14 - km 163,5 in Area Science Park, 34149 Basovizza, Trieste, Italy.

[d] Lund Universitet, MAX-lab, Ole Römers väg 1, SE-223 63 Lund, Sweden.

[e] Laboratory of Photonics and Interfaces, Institute of Chemical Science and Engineering, Faculty of Basic Science, Ecole Polytechnique Fédérale de Lausanne, CH-1015 Lausanne, Switzerland.

‡ Present address: School of Chemistry, The University of Nottingham, University Park, Nottingham, NG7 2RD, UK

AUTHOR EMAIL ADDRESS

a.g.thomas@manchester.ac.uk

RECEIVED DATE (to be automatically inserted after your manuscript is accepted if required according to the journal that you are submitting your paper to)

ABSTRACT

Photoemission and near-edge X-ray absorption fine structure (NEXAFS) techniques have been used to study the adsorption of pyrocatechol on anatase TiO_2 (101) and rutile TiO_2 (110) single crystals. Photoemission results suggest the pyrocatechol molecule adsorbs on both surfaces predominantly in a bidentate geometry. Using the searchlight effect, the carbon K-edge NEXAFS spectra recorded for pyrocatechol on anatase TiO_2 (101) and rutile TiO_2 (110) show the phenyl rings in the pyrocatechol molecule to be oriented at 27°±6° and 23°±8° respectively from the surface normal. Experimental data and computational models of the pyrocatechol-anatase TiO_2 interface indicate the appearance of new occupied and unoccupied states on adsorption due to hybridisation between the electronic states of the pyrocatechol molecule and the surface. The atomic character of the new orbitals created facilitates direct photoinjection from pyrocatechol into anatase TiO_2 and induces a strong final state effect in the carbon K-edge NEXAFS spectrum.

1. Introduction

TiO_2 is of technological interest for applications such as photocatalysis, self-cleaning surfaces, biomaterials and novel photovoltaic solar cells[1-4]. Many of these applications use TiO_2 in a nanoparticulate form. Functionalised TiO_2 nanoparticles have been investigated for biological and environmental applications such as bioelectronics, anti-fouling materials and for killing bacteria[5-8]. Nanoparticulate TiO_2 is used as an n-type semiconductor in dye sensitised solar cells (DSSCs). TiO_2

absorbs light in the UV region of the spectrum, so the nanoparticle surfaces are coated with an organic molecule (the dye) which absorbs light in the visible region of the spectrum to optimize absorption of the solar spectrum[2,9,10].

Titanium dioxide has three polymorphs, rutile, anatase and brookite. TiO_2 nanoparticles generally adopt the anatase structure[11]. However, single crystals of anatase TiO_2 are difficult to grow using traditional methods and, with a few notable exceptions[12-14], clean, well-characterised surfaces are difficult to prepare on natural crystals in ultrahigh vacuum (UHV). Some small high quality single crystals grown by a chemical transport method[15] are available and a few studies of the (101) and (001) surfaces have been carried out[10,16-20] In addition, there are some studies of thin film anatase surfaces grown on $SrTiO_3$ substrates[21-23]. Large rutile single crystals, on the other hand, are readily commercially available and therefore have been studied more widely[24,25]. Anatase (101) and rutile (110) are crystallographically equivalent surfaces, both cut down the longest diagonal plane of their respective unit cells. Here we determine the adsorption geometries of pyrocatechol on both single crystal anatase (101) and rutile (110) surfaces.

Pyrocatechol (also known less specifically as 'catechol') is shown in figure 1(a). It is of interest as a light-harvesting molecule for solar cells when adsorbed on TiO_2[26]. Pyrocatechol does not absorb light of energy below 4.1 eV (300 nm) which is much larger than the 3.2 eV band gap of TiO_2[27]. However, when pyrocatechol is adsorbed onto nanoparticulate TiO_2 (figure 1(b)), the onset of absorption is around 3 eV (420 nm)[27]. A similar absorption shift has been found for other catechol-based molecules[28]. It has been hypothesized that the mechanism of charge transfer from the molecule to the TiO_2 surface in this system differs from that in DSSCs. In the DSSC system, the sensitizing dye molecules absorb the incident sunlight and a photon excites an electron from the ground state of the dye into an unoccupied state. The dye is then in an excited state. The excited electron is then rapidly injected into the TiO_2 conduction band on a femtosecond timescale[29]. In the case of the catechol-TiO_2 system, Persson *et al*.[27] propose that

instead of electron excitation in the adsorbate followed by injection into the TiO_2 conduction band, the electron is directly photoinjected from the ground state of the catechol into the TiO_2 substrate. This means that the electron is transferred from the adsorbate into the substrate without the participation of excited states in the catechol molecule. In this model, the direct charge transfer takes place by excitation from the highest occupied π orbital in the catechol molecule to the Ti^{4+} (3d) levels at the bottom of the conduction band of the TiO_2[27]. It is therefore of considerable interest to investigate the new occupied and and unoccupied states that are formed on adsorption of pyrocatechol on TiO_2. While a number of modelling studies of this interface have been carried out[27,30-33], experimental data are rather more scarce. An elegant photoemission and STM study of the occupied states has been made by Li *et al*.[13,34]. Here, we complement this work with a detailed study of the unoccupied states by NEXAFS, and also use this to infer the adsorption geometry.

There are three possible structures that pyrocatechol may adopt when adsorbed onto a TiO_2 surface; (1) a bridging bidentate structure, where each oxygen atom is bonded to a different titanium atom on the surface; (2) a chelating bidentate structure, where both oxygen atoms are bonded to the same titanium atom on the surface; (3) a monodentate structure, where only one of the oxygen atoms is bonded to a titanium atom on the surface. Figure 1 (c) shows a schematic picture of these three structures. Redfern *et al*.[32] carried out a theoretical study of pyrocatechol adsorption on anatase TiO_2 and determined that on a stoichiometric anatase TiO_2 surface, pyrocatechol adsorbs in a bridging bidentate geometry, while a chelating bidentate structure is favoured when adsorption occurs at a defect site (containing a Ti=O moiety). A bidentate geometry is also adopted in the modeling work of Persson *et al*.[27] and Rego and Batista[45]. The presence of predominantly bridged bidentate species (with some chelating bidentate species) is suggested from measurements made in aqueous solution[33]. Dopamine (a related catechol) has been shown to adsorb on anatase (101) in a bidentate tilted geometry[17]. Li *et al*.[13,14,34] have used scanning tunneling microscopy (STM) and angle-resolved ultraviolet photoemission spectroscopy to study pyrocatechol adsorbed on rutile TiO_2 (110) and anatase (101) surfaces. These authors deduced that

adsorbate-induced band gap states on rutile TiO_2 (110) are only observed when pyrocatechol is adsorbed in a bridging bidentate geometry. They propose that pyrocatechol adsorbs on the rutile TiO_2 (110) surface in a mixed monolayer coverage of both monodentate and bridging bidentate structures that can easily convert into a fully-monodentate coverage via proton exchange between the pyrocatechol and the surface. Using angle-resolved UPS they calculate that the pyrocatechol molecules that give rise to the band gap state are tilted by ±15-30° from the surface normal. The more recent STM measurements/DFT calculations for the anatase (101) surface by the same authors indicate that at low coverages the monodentate and bidentate configurations have similar energies, but that the bidentate configuration is stabilized at high coverage by attractive intermolecular interactions[14].

In this paper, core and valence band photoemission results for pyrocatechol adsorbed on single crystal anatase TiO_2 (101) are presented. These are compared to corresponding results for the same molecule adsorbed on the crystallographically-equivalent rutile TiO_2 (110) surface. Core level photoemission allows us to conclude that the mode of adsorption is primarily bidentate on both surfaces at saturation coverage. We study the unoccupied states using C K edge NEXAFS spectroscopy, which is also used to determine the orientation of the pyrocatechol molecule at the TiO_2 surfaces. The experimental filled and empty state measurements are compared with Density Functional Theory (DFT) geometry optimisations of the isolated pyrocatechol molecule and of the molecule adsorbed on an anatase TiO_2 (101) cluster. New unoccupied states are found to appear as a result of hybridization between the electronic states of the pyrocatechol molecule and the anatase surface. The DFT calculations for the ground state are then used as the starting point for simulation of the NEXAFS spectra, incorporating the effects of the core hole. The new unoccupied states give rise to a strong final state effect in the C K-edge NEXAFS, and this is found to be reproduced in our experiment. We identify new unoccupied states that can facilitate charge transfer between pyrocatechol and the anatase surface. The adsorbate-induced modification of

the surface electronic structure is used to rationalize the experimental optical absorption of the pyrocatechol/anatase system.

2. Methods

a. Experimental procedures

This work was carried out on beamline BACH ($35 \leq h\nu \leq 1600$ eV) at the synchrotron facility Elettra in Italy, and beamline D1011 ($30 \leq h\nu \leq 1500$ eV) at MAX-lab in Sweden. The BACH endstation is fitted with a VSW 150 mm mean radius hemispherical electron energy analyser. The D1011 endstation is equipped with a SCIENTA SES200 200 mm mean radius hemispherical electron energy analyser and a microchannel plate (MCP) NEXAFS detector. The anatase TiO_2 crystal (approximately 3 mm x 3 mm) was grown by a chemical transport method[15]. It was mounted by wrapping in a Ta strip, which was then spot welded across the sample plate. The rutile TiO_2 crystal (Pikem Ltd.) was cut and epi polished on one side to within 0.2° of the (110) plane. A thermocouple was attached to the crystals to allow the sample temperature to be monitored during the experiment. The crystals were cleaned by repeated 1 keV Ar^+ ion etching and annealing to 750 °C in vacuum until XPS spectra showed no contamination and sharp (1 x 1) LEED patterns were obtained[35].

To evaporate pyrocatechol onto the TiO_2 crystals, pyrocatechol powder (≥99.5%, Fluka) was packed into a tantalum envelope in a house-built evaporator. The powder was degassed prior to use by heating the tantalum envelope in the evaporating arm. When evaporating pyrocatechol into the chamber the tantalum envelope was heated to 30-40 °C. Dosing times of between 8 and 22 minutes had no influence on the coverage achieved as determined from the relative intensity of pyrocatechol and TiO_2-derived O 1s photoemission peaks. This corresponds to saturation coverage of 1 ML (one monolayer), meaning

one catechol molecule is adsorbed on the surface per two TiO_2 unit cells[13,14,34]. No evidence of multilayer formation was observed. Similarly, no multilayer formation was observed by Li *et al.*[13,34]. Using STM these authors found that pyrocatechol forms an ordered densely packed monolayer on the rutile (110) and anatase (101) surfaces.

Photoemission spectra were recorded at normal emission with the incident beam at 60° to the surface normal at BACH and 40° to the surface normal at D1011. Core level spectra were recorded with photon energies of 700 eV or 1000 eV at D1011, and 590 eV at BACH. Clean and dosed spectra were aligned on the binding energy scale using Fermi edges recorded from the tantalum sample clips and binding energies are quoted to ±0.1 eV. The NEXAFS spectra at BACH were recorded by detecting C Auger electrons at a kinetic energy of 260 eV using the hemispherical electron analyser. At D1011 the NEXAFS spectra were recorded in partial yield mode using an MCP NEXAFS detector. Peak fitting was performed using CasaXPS software. A Shirley background was subtracted from the data. Voigt curves (70% Gaussian:30% Lorentzian) were used to fit the core level spectra.

b. Computer modelling

Computer modelling was carried out using Gaussian '03[36] and StoBe-deMon[37]. Geometry optimisations and molecular orbital calculations of the ground state of the isolated pyrocatechol molecule and the pyrocatechol molecule adsorbed on an anatase TiO_2 (101) cluster were performed using Gaussian '03. Excited state calculations to simulate NEXAFS spectra were performed using StoBe-deMon.

The geometry optimisation of the pyrocatechol molecule was carried out using Gaussian '03 with a DFT B3LYP theory and a 6-31G (d, p) basis set. The coordinates of the geometry-optimised molecule were then used by StoBe to perform an excited state calculation, incorporating the effects of the core

hole, and to simulate a NEXAFS spectrum. The six carbon atoms (numbered in figure 1) were simulated separately, energy calibrated and then added together to produce the total NEXAFS simulation. Each simulated NEXAFS spectrum corresponds to an angular average, *i.e*. as if obtained from an ensemble of molecules that are randomly orientated with respect to the electric field vector.

To model the pyrocatechol molecule adsorbed on the anatase TiO_2 (101) surface, a cluster of 5 titanium atoms was used, as shown in figure 1(b). Hydrogen saturators were used on oxygen atoms with dangling bonds and DFT theory with a B3LYP exchange correlation functional and a 6-31G basis set were used for the geometry optimisation. Based on results from XPS (section 3) a bridging bidentate geometry was used to allow comparison with our experimental data. The coordinates of the atoms in the TiO_2 cluster were kept frozen during the calculation except for the two titanium atoms that the pyrocatechol molecule is bonded to and the oxygen atom between these two titanium atoms. Coordinates from the pyrocatechol molecule-TiO_2 anatase cluster were then transferred into StoBe to generate a NEXAFS spectrum as for the isolated molecule

3. Results

To study the adsorption of pyrocatechol on anatase TiO_2 (101), photoemission spectra were measured from the clean surface and again following evaporation of pyrocatechol. These measurements were repeated on the rutile TiO_2 (110) surface for comparison. Figure 2(a) shows the O 1s spectrum for clean anatase TiO_2 (101), 1 ML pyrocatechol adsorbed on anatase TiO_2 (101), clean rutile TiO_2 (110) and 1 ML pyrocatechol adsorbed on rutile TiO_2 (110). Peak assignments and relative abundances of the surface species are shown in table 1.

In the spectra of clean anatase and clean rutile there are single peaks at 530.9 eV and 530.4 eV binding energy (BE) respectively. These peaks arise from the oxygen atoms in the TiO_2 crystal[38]. The absence of

any significant higher binding energy components shows that there is very little contamination on the surfaces. Following adsorption of pyrocatechol, the most intense peak at 530.8 eV BE (530.0 eV for rutile) corresponds to oxygen atoms in the TiO_2 surface[38]. The peak at 531.9 eV BE (531.3 eV for rutile) originates from the oxygen atoms in the pyrocatechol molecule following deprotonation and adsorption on the surface as C-O-Ti (by analogy with the adsorption of carboxylic acids on TiO_2 surfaces)[39]. The appearance of only one strong peak after adsorption suggests pyrocatechol adsorbs at high coverage on both surfaces predominantly in a bidentate geometry, where both pyrocatechol O atoms are chemically equivalent, as found for bi-isonicotinic acid (BINA) adsorption on anatase (101) and rutile (110) surfaces[19,40]. (Clearly here we have only two points of attachment whereas for di-carboxylic acid anchor groups of TiO_2-sensitizing dyes including BINA[19,40] and maleic anhydride[41] there are four points of attachment to the surface, which arise from the presence of two carboxylic acid groups.) The small third peak at 532.8 eV BE (532.9 eV for rutile) is likely to be from hydroxyl (OH) groups[39]. This could be from contamination during dosing or from protons lost from pyrocatechol upon adsorption and now adsorbed on the TiO_2 surface. It could also arise from molecules that are adsorbed in a monodentate geometry, *i.e.* one OH group in the pyrocatechol molecule becomes deprotonated and bonds to the surface and one OH group stays intact. However, this third peak is too small to suggest that all the pyrocatechol molecules adsorb in a monodentate geometry since this scenario would give rise to two adsorbate O 1s peaks of equal intensity. A mixed monodenate-bidentate coverage with equal numbers of bidentate and monodentate structures would give a ratio of 3:1 for the peaks assigned to C-O-Ti:C-OH. In this study, the two peaks that appear following adsorption of pyrocatechol on rutile TiO_2 (110) give a ratio of approximately 6:1. This gives a minimum of 2.5 bidentate structures for each monodenate structure in the limit where no surface OH is present. Following adsorption on anatase TiO_2 (101) this ratio is approximately 4:1, so here a mixed monodentate-bidentate coverage with a maximum of 0.7 monodentate molecules per bidentate molecule is possible if no surface OH is present. Since the hydroxyl peak is small and very likely to include a significant contribution from surface OH bonded to Ti, the data suggest that pyrocatechol adsorbs onto these TiO_2 surfaces at saturation coverage primarily

through both oxygen atoms, but we note that these data alone do not allow us to distinguish between chelating bidentate or bridging bidentate geometries. However, recent work supports the bridging bidentate geometry for five-fold-coordinated surface Ti[14]. Following adsorption of pyrocatechol the O 1s signal from the TiO_2 crystal was found to shift to lower binding energy in both anatase and rutile spectra. The peak shifted by 0.1 eV on the anatase crystal and 0.4 eV on the rutile crystal. Similar shifts have been observed for dopamine adsorption on anatase TiO_2 (101)[17] and are discussed further below.

Figure 2(b) shows the C 1s spectra following adsorption of 1 ML pyrocatechol on anatase TiO_2 (101) and rutile TiO_2 (110). Peak assignments are shown in Table 2. The peak at lower binding energy is assigned to carbon atoms 3-6 in the pyrocatechol molecule (see figure 1 for numbered carbon atoms)[14,42,43]. The peak at higher binding energy is due to carbon atoms 1 and 2 in the pyrocatechol molecule, which are bonded to the surface through the pyrocatechol oxygen atoms and thus deshielded relative to carbon atoms 3-6, resulting in a significant chemical shift[14,42,43]. The area ratio of these peaks is 2:1 as is expected, indicating the catechol molecule is adsorbed intact. The two peaks are separated by 1.5 eV and 1.4 eV in the anatase and rutile spectra respectively. This agrees with a study by Weinhold *et al*.[42] of L-DOPA (a related molecule) on gold where the signals from the aromatic carbon atoms and the carbon atoms attached to the hydroxyl groups are separated by 1.6 eV. The observation of a larger chemical shift for anatase than for rutile suggests that pyrocatechol is somewhat more strongly bound to the anatase surface than to the equivalent rutile surface.

Figure 2(c) shows the corresponding Ti 2p spectra. Peak assignments are shown in Table 3. The two fitted peaks in the anatase spectra arise from surface Ti^{4+} atoms in the anatase crystal and correspond to the spin-orbit-split $2p_{3/2}$ and $2p_{1/2}$ components respectively[44]. The rutile spectra are fitted with Ti^{4+} spin-orbit-split peaks at similar binding energies to the anatase spectra. The components were constrained to give approximately a 2:1 ratio of $2p_{3/2}$:$2p_{1/2}$ peak intensity. The small spin-orbit-split peaks at binding

energies of 457.3 eV and 463.0 eV BE in the clean rutile spectrum are due to Ti^{3+} states[45] arising from surface oxygen vacancies[46] created by annealing. In comparison, no feature arising from Ti^{3+} is observed in the spectra recorded from the similarly-prepared anatase (101) surface. Following adsorption of pyrocatechol the Ti 2p peaks are shifted to lower binding energy. The substrate Ti 2p peaks (Ti^{4+}) shift by approximately 0.1 eV for anatase and 0.2 eV for rutile. These shifts correlate approximately with the shifts observed in the O 1s spectra following adsorption of pyrocatechol. The peaks associated with Ti^{3+} in the clean rutile spectra are attenuated relative to those due to Ti^{4+} following adsorption of pyrocatechol on the rutile surface. This suggests that Ti^{3+} is re-oxidised to Ti^{4+} as the pyrocatechol binds to it via the deprotonated oxygen atoms. Similar observations have been reported by Wang *et al.*[47], where small molecules (N_2O, O_2 and H_2O) were found to 'heal' a defected TiO_2 (110) surface. These authors found a reduction in intensity in the shoulder of the Ti 2p spectrum assigned to Ti^{3+} and a corresponding reduction in the intensity of a state in the band gap associated with d^1 states on adsorption[47].

The core-level binding energy shifts on adsorption are replicated in valence band photoemission (discussed below) and may be explained by a reduction in band bending at the surface following adsorption of pyrocatechol. Similar effects have been observed following dopamine adsorption on rutile TiO_2 (110)[17]. Removing surface defects associated with Ti^{3+} reduces the amount of band bending that is present on the clean surface. There is no evidence of Ti^{3+} in the case of the anatase (101) surface and the shifts observed for anatase are correspondingly smaller than in rutile.

Figure 3 shows the valence band spectra for (a) clean rutile TiO_2 (110) and 1 ML pyrocatechol adsorbed on rutile TiO_2 (110) and (b) clean anatase TiO_2 (101) and 1 ML pyrocatechol adsorbed on anatase TiO_2 (101). The valence band spectrum of pyrocatechol adsorbed on rutile is recorded with the electric vector, E, of the incident light parallel to the [001] direction. The main valence band structure in the clean anatase spectrum has peaks at 5.9 eV and 7.6 eV BE while the clean rutile spectrum has

peaks at 5.7 eV and 8.2 eV BE. The main structure of the valence band arises from O 2p states with some Ti 3d and 4sp character. The peak at 22.8 eV BE arises from O 2s states. Both spectra are consistent with published work[35,48]. The clean rutile spectrum shows a small peak at 1 eV BE indicating the presence of surface defects[35,46,48]. This 'defect' peak has long been attributed to the occupation of Ti 3d states following the creation of Ti^{3+} (d^1) at the surface[24,49-51], thought to arise from the removal of oxygen in so-called 'bridging' sites[46,48]. This agrees with the Ti 2p spectrum recorded from the clean rutile TiO_2 (110) surface (figure 2(c)) which indicates the presence of Ti^{3+} species. This peak has also been associated with hydroxylated O-vacancies[46] or Ti interstitials in the near-surface region[52]. The anatase spectrum indicates that there is a low number of defect states on the anatase surface since there is no peak in the band gap at around 1 eV BE, arising from oxygen vacancies. This is in agreement with the Ti 2p spectrum (figure 2(c)) where no peaks arising from Ti^{3+} are observed. We note that oxygen vacancies have been shown to occur predominantly in the subsurface layers at the anatase (101) surface[12]

Adsorption of pyrocatechol on the anatase surface leads to a number of new peaks appearing in the valence band spectrum between 2.6 eV and 25.2 eV BE; similar features are observed following pyrocatechol adsorption on rutile. The 'defect' feature at 1.0 eV binding energy observed on the clean rutile surface is reduced in relative intensity following adsorption of pyrocatechol. This indicates that some of the Ti^{3+} observed on the clean surface is removed by the adsorption of the pyrocatechol. This is consistent with the Ti 2p spectra (figure 2(c)) where the shoulder in the clean spectrum arising from Ti^{3+} is reduced in relative intensity following adsorption of pyrocatechol. Figure 3(c) shows the valence band difference spectra for 1 ML pyrocatechol adsorbed on anatase and rutile. These were generated by subtracting the clean TiO_2 surface spectrum from the 1 ML pyrocatechol-dosed TiO_2 spectrum (after accounting for the band-bending shift between clean and dosed spectra). The StoBe-calculated density of states spectrum of an isolated pyrocatechol molecule is shown in the figure for comparison. This was calculated using the coordinates of the optimised pyrocatechol molecule from Gaussian obtained using

triple zeta and valence polarization (TZVP) basis sets. The StoBe simulation was shifted by 1.8 eV to lower binding energy to match the features in the experimental difference spectrum on anatase, aligning the high binding energy peaks at around 13 eV, 17 eV and 20 eV. To match the features in the rutile spectrum a shift of 2.2 eV to lower binding energy is needed. This shift indicates the relaxation/polarisation shift upon adsorption. This is the binding energy difference between the orbitals of the gas phase molecule (in this case, the calculation) and those of the adsorbed molecule. This shift occurs because the final state in photoemission is screened by the presence of the surface[53]. The StoBe-calculated features agree well with the difference spectrum for the anatase system but not as well for the rutile system. The feature in the rutile difference spectrum at 4.7 eV is very intense compared to the StoBe calculation and the anatase difference spectrum, suggesting a residual element of the substrate valence band spectrum remains. Similarly the O 2s core level feature at around 23 - 25 eV BE is broad, suggesting it contains contributions from both the pyrocatechol molecule and the substrate. In the case of anatase, the difference spectrum is aligned well with the calculated O 2s core level feature of the pyrocatechol molecule at 25.2 eV BE. It can be seen that adsorption of pyrocatechol induces a new feature in the band gap of both surfaces with a maximum at 2.6 eV BE, in good agreement with the work of Li *et al*.[13,34]. Alignment of the high binding energy features of the calculated and experimental data reveals that the HOMO of the adsorbate system is shifted by 1.2 eV to low BE relative to the unbound molecule (marked by the dotted line in figure 3), in good agreement with the substantial shift predicted for bidentate adsorption by the modeling work of Redfern *et al*.[32]. We assign the atomic character of the valence band states partly through reference to related systems (such as phenol adsorbed on semiconductor surfaces[54]) as follows. The features at 2.6 and 4 eV binding energy are mainly of C π character, while the larger feature at 7.7 eV BE is likely to have mixed C σ and fairly localized O 2p character. The feature at 10.5 eV BE has σ O-H character. Features to higher binding energy are more 'core-like', with significant C 2s and O 2s character.

Figure 4 shows the carbon K edge NEXAFS spectra of 1 ML pyrocatechol adsorbed on anatase TiO_2 (101) for incident radiation angles of 30° to 90° to the surface (measured on beamline BACH at Elettra). The spectra are first normalised to remove photon-flux and substrate-induced features by dividing the pyrocatechol-dosed TiO_2 carbon K edge NEXAFS spectrum by the corresponding clean anatase spectrum. The resulting spectrum was then normalised by setting the height of the step edge (the increase in intensity as the ionization potential is passed) to unity. The peak at 285.7 eV photon energy (π_a* in figure 4) arises from excitations from the C 1s level into the π* orbitals of carbon atoms 3-6 (carbon atoms not bonded to oxygen atoms)[55] and the peak at 287.2 eV (π_b*) originates from C1s → π* excitations for carbon atoms 1 and 2 (carbon atoms bonded to oxygen atoms)[55]. These peaks have an area ratio of approximately 2:1 as expected. The spectra also show an additional feature at lower photon energy than the primary π* peak, at around 283 eV. The origin of this feature is discussed in more detail below. Figure 4 also shows the carbon K edge NEXAFS spectra of 1 ML pyrocatechol adsorbed on rutile TiO_2 for incident radiation angles of 20° to 90° to the surface (measured on beamline D1011 at MAX-lab). The spectra are normalised using the same method. Here the π_a* peak is at 285.4 eV and the π_b* peak is at 287.3 eV photon energy. The feature at 283 eV observed for anatase is absent. A Ti L edge spectrum recorded from the clean surface was used to align the spectra on the photon energy scale.

Gaussians and a step edge were fitted to each individual spectrum to produce the best fit to the data as indicated in figure 4. The Gaussian peaks fitted to the spectrum arise from the main π* and σ* resonances. The areas of the π_a* peaks are plotted as a function of photon incidence angle to the surface in the insets in figure 4. The C 1s -> π_a* intensity is a maximum when the direction of the electric vector of the incident synchrotron radiation is aligned with the axis of the unoccupied orbital. Algorithms which describe the effect of the symmetry of the surface and the nature of the unoccupied orbital on this intensity have been developed and are described in detail by Stöhr[56]. In this case we have used the equations for a surface with two-fold rotational symmetry and a vector-like unoccupied orbital as

described in ref 56. The graphs in figure 4 are normalised so that the point with the largest intensity π_a* peak has intensity equal to 1 and the Stöhr equations[56] are fitted to the data, from which the angle between the π_a* orbital and the surface normal is obtained. For pyrocatechol adsorbed on anatase, this indicates that the π* orbitals lie 63°±6° away from the surface normal. The plane of the aromatic ring (defined by the σ* orbitals) is perpendicular to the π* orbitals so is oriented at 27°±6° from the surface normal. For pyrocatechol adsorbed on rutile, the corresponding angle for the plane of the aromatic ring is 23°±8° from the surface normal. Li *et al*.[34] found catechol molecules on rutile TiO_2 (110) to be tilted by ±15-30° from the surface normal using angle resolved UPS so these results are consistent with their study. The angles obtained for the anatase and rutile surfaces are the same within experimental error. This is not surprising since the NEXAFS searchlight technique has previously revealed that the adsorption geometries for bi-isonicotinic acid adsorbed on anatase (101) and rutile (110) are similar[19,40].

The main features of the NEXAFS spectra presented in figure 4, like the C K-edge spectra of other phenyl-ring-containing adsorbates on TiO_2[19,57] are relatively straightforwardly assigned as described above. However, in the case of the anatase (101) surface, an additional feature at lower photon energy than the primary π* peak is observed at approximately 283 eV photon energy (figure 4); the origin of this is not immediately obvious. The variation in intensity of this feature with angle suggests it has π* character. In order to better understand this feature, we have simulated the NEXAFS spectra, beginning with the spectrum expected from unbound pyrocatechol molecules. Figure 5 shows the comparison between the StoBe-calculated angle-integrated NEXAFS spectrum of pyrocatechol and the experimental NEXAFS spectrum of pyrocatechol adsorbed on anatase TiO_2 (101) recorded at normal incidence. The StoBe NEXAFS spectrum was shifted by 0.89 eV to higher photon energy to align with the experimental π* peaks. The intensities of the π* and σ* peaks relative to each other give us little information since the intensities of the experimental peaks change with the photon incidence angle while the StoBe-generated spectrum is effectively an angle-integrated spectrum (*i.e*. as if the molecules

were randomly oriented relative to the incident radiation). However, over the region of the two π* peaks there is a reasonable fit to the experimental data. The overall shape of the StoBe-generated spectrum is similar to the experimental data but the calculated σ* features are at a much lower energy than in the experimental spectra. In addition, the peak at 283 eV is not reproduced in the calculation for the isolated pyrocatechol molecule.

The discrepancies between our experiment and the calculated NEXAFS for the isolated pyrocatechol molecule are therefore likely to reflect changes in the electronic structure of the unoccupied states that take place when pyrocatechol binds to the anatase (101) surface. We investigated this by modelling the adsorbate-substrate interaction. A cluster of 5 titanium atoms was used and the molecule was adsorbed in a bridging bidentate geometry on the cluster as discussed in section 2. This approach was adopted by Redfern *et al*. in their calculations of pyrocatechol adsorption on anatase TiO_2 surfaces[32], and is supported by the O 1s spectra of figure 2(a), which suggest that the majority surface species is bidentate. A number of other studies also suggest that a bridging bidentate structure is more likely than monodentate adsorption on the anatase (101) surface at saturation coverage[34]. Figure 1(b) shows the geometry-optimised cluster of pyrocatechol on the anatase surface. The phenyl ring of the adsorbed pyrocatechol molecule is found to tilt at an angle of 42° from the anatase surface normal. Experimentally the angle of the phenyl ring of the pyrocatechol molecule was found to be approximately 27°±6° from the surface normal. The calculation therefore gives a somewhat larger tilt angle from the surface normal than is observed. This is likely to be because the calculation is performed for an isolated pyrocatechol molecule adsorbed at a small TiO_2 cluster, whereas experimentally we have studied a closely-packed overlayer where the molecules are likely to adopt a more upright configuration. With this caveat, the agreement between experiment and modelling is reasonably good.

Figure 6 shows electron density distribution isosurfaces for the HOMO and LUMO of the isolated pyrocatechol molecule and the pyrocatechol molecule adsorbed on an anatase TiO_2 (101) cluster calculated by Gaussian '03[36]. The red and green areas correspond to +/- phases of the isosurfaces. The HOMO of the cluster is primarily located on the pyrocatechol molecule. This molecular orbital is very similar to the HOMO of the isolated pyrocatechol molecule. However, the LUMO of the cluster is primarily located on the TiO_2 surface rather than the pyrocatechol molecule. In this combined 'surface + adsorbate' system excitation of an electron from the HOMO (of C π character) to the LUMO would effectively result in its direct transfer from the pyrocatechol molecule to the anatase surface, in the scenario suggested by Persson *et al.*[27]. A very similar electronic structure is observed for doubly protonated *cis*-(dithiocyanato)-Ru-*bis*(2,2'-bipyridine-4,4'-dicarboxylate), known as N719, adsorbed on an anatase TiO_2 nanoparticle[58]. Here, modelling shows that the HOMO is located on the N719 dye but the LUMO is located on the TiO_2 surface[58].

Isosurfaces for the low-lying LUMOs of the pyrocatechol-on-anatase cluster (up to LUMO+10) are shown in figures 6 and S1 (Supporting Information). The LUMO+1, LUMO+2 and LUMO+4 states are also more localised on the TiO_2 surface than the pyrocatechol molecule, but have some density on the molecule (in the case of LUMO+1, mainly on C_3 and C_6, and for LUMO+2 and LUMO+4 on $C_{1,2}$ and the associated oxygen atoms. Here the subscripts refer to the carbon atom labels in figure 1a). This would be expected to increase the oscillator strength of direct transitions from the HOMO, facilitating direct photoinjection from pyrocatechol to the TiO_2 surface as predicted by Persson *et al.*[27]. The LUMO+3 and LUMO+5 orbitals are entirely localized on the TiO_2 surface. The first molecular orbital above the HOMO that is located very appreciably on the pyrocatechol molecule was found to be the LUMO+6 (figure 6). This molecular orbital is located partly on the anatase surface and partly on the molecule. The LUMO+7, also shown in figure 6, was found to be predominantly located on the pyrocatechol molecule and is similar to the LUMO of the isolated molecule. The energies (from

Gaussian '03) of the HOMO and LUMO+7 of the pyrocatechol-on-anatase cluster coincide approximately with the energies of the HOMO and LUMO of the isolated pyrocatechol molecule suggesting that the LUMO to LUMO+6 of the cluster are new states formed by bonding between the molecule and the surface. The LUMO of the cluster lies *ca*. 0.6 eV below the LUMO+7. The calculations for catechol bound to a hydrated Ti^{4+} ion in solution by Duncan *et al*.[30] also show that the HOMOs of free and bound pyrocatechol are similar but the molecular orbital that matches the LUMO in the free molecule is the LUMO+8 in the bound molecule (in the cluster model presented here, the LUMO+8 is located in the surface, figure S1). A similar effect was found for the N719 dye adsorbed on an anatase TiO_2 nanoparticle[58]. De Angelis *et al*. investigated various adsorption geometries and found that the shifts in energy on bonding may be so large that the LUMO of the unbound dye corresponds to the LUMO+6 - LUMO+8 of the combined dye-anatase TiO_2 system.

The geometry optimisation of pyrocatechol adsorbed on the small anatase cluster gives new bond lengths and relative coordinates of the atoms in the molecule compared to the isolated pyrocatechol molecule. These new coordinates are expected to give a better model of the experimental pyrocatechol-anatase interface. By taking these new coordinates and repeating the StoBe NEXAFS simulation, a more realistic simulated spectrum can be produced. We note at this point that while the Gaussian '03 calculations give ground state orbital energies and isosurfaces, StoBe NEXAFS simulations take into account the presence of the core hole in the final state, producing excited state spectra. In figure 5 the resulting StoBe-generated simulated NEXAFS spectrum for the pyrocatechol-on-anatase cluster is compared with the experimental C K-edge NEXAFS for pyrocatechol adsorbed on anatase TiO_2 (101) (taken at normal incidence). The total NEXAFS spectrum was shifted by 0.81 eV to higher photon energy to align with the π* peaks of the experimental data. The π* resonances in the calculated spectrum now give a significantly better agreement with the experimental data than the calculation using the isolated pyrocatechol molecule; the π_a^*-π_b^* spacing is now very accurately reproduced, as are the

relative intensities. This suggests the bonding geometry (bridging bidentate) in the cluster calculation is realistic. However, the calculation still predicts the σ* resonances to occur at too low an energy. More significantly, the calculated spectrum now shows a double-peaked feature at lower binding energy than the main π* resonance (at approximately 283 eV) that was not present in the calculation for the isolated pyrocatechol molecule. This lies at a similar energy to the anomalous low photon energy feature observed in the experimental NEXAFS. These peaks must therefore have their origin in the bonding of the pyrocatechol molecule to the anatase surface. In order to be observed strongly in the C K-edge NEXAFS in this geometry the final states involved must have some carbon π* character. However, it is not possible to identify the new spectral features straightforwardly with the LUMO – LUMO+6 orbitals produced by the ground state Gaussian '03 calculation. In order to assign the features we must consider final state effects, described below.

As discussed earlier, the main π* resonance of the NEXAFS spectrum (at around 286 - 287 eV) is split into two peaks by initial state effects, arising from the chemical shift between the environments of carbon atoms 1,2 and 3-6. The simulated NEXAFS spectrum for the pyrocatechol-on-anatase cluster (figure 5) shows that the new feature echoes this structure, but is separated from the main π* resonance by 3 eV. As it appears at a photon energy of 283 eV, lower than the corresponding C 1s binding energy (figure 2), it is immediately apparent that it must be attributed to final state effects. If we identify the main π* resonance at 286 eV with the LUMO+7 of the ground state Gaussian '03 calculations, we similarly note that the 283 eV feature cannot be identified with the ground state energies of LUMO – LUMO+6, all of which lie within 0.6 eV of the LUMO+7 energy. In fact final state effects in the NEXAFS of small aromatic molecules, particularly those containing inequivalent carbon atoms, are well-known and large[59,60]. Splitting of the π* resonance can occur, caused by screening effects due to the excitonic character of this excitation. In general, the NEXAFS of such molecules cannot be directly related to the density of unoccupied states obtained from a ground state calculation[59]. Following the

creation of a C 1s core hole in the NEXAFS process, the unoccupied molecular orbitals (UMOs) are stabilized by the additional Coulomb interaction to differing degrees, depending upon their overlap with the C 1s orbital of the excited carbon atom. This is turn depends on their initial energy and atomic character, and results in significant reordering of the orbital energies from the ground state. UMOs that contain a large contribution from the excited atom may be stabilized by several eV, and the lowest energy UMOs are preferentially stabilized as the overlap between the initial and final states is generally largest for the lowest energy orbitals[59]. In the present case, we expect any of the new low energy states arising from the bonding between the pyrocatechol molecule and the anatase surface (LUMO – LUMO+6) to be strongly preferentially stabilised if they have some C π* character on the excited C atom. By examining the LUMOs shown in figures 6 and S1, we find that this is the case for the $C_{1,2} \rightarrow$ LUMO+2,4 and $C_{3\text{-}6} \rightarrow$ LUMO+1 transitions. In the simulated NEXAFS spectrum, we assign the feature at 282.9 eV photon energy to $C_{3\text{-}6} \rightarrow$ LUMO+1, that at 283.9 eV photon energy to $C_{1,2} \rightarrow$ LUMO+2, with the $C_{1,2} \rightarrow$ LUMO+4 transition underlying the main π* resonance. Thus the LUMO+1 and LUMO+2 formed when the pyrocatechol molecule binds to the anatase (101) surface give rise to the new structure in the NEXAFS spectrum through strong stabilization of the core-hole final states.

We have attempted to replicate this calculation for the rutile (110) surface, where we do not observe additional final state structure in the experimental NEXAFS spectrum (figure 4). A larger cluster size is required to replicate the features of this surface than for anatase (101). Geometry optimisations were attempted using several cluster models, but convergence was not obtained for any. It is therefore not clear at present why the 283 eV feature is absent in the case of rutile (110), although we note that XPS suggests that the pyrocatechol molecule is somewhat more strongly bound to the anatase (101) surface than to rutile (110). As it is clearly the interaction between the molecule and the TiO_2 surface, which gives rise to the final state effect in the NEXAFS spectrum, then its presence or absence is most likely related to the strength of the bonding. Further work, examining the calculated and

experimental Ti and O unoccupied density of states (e.g the O 1s and Ti 2p XAS) is required to clarify this point.

Figure 7 shows a schematic energy band diagram of the pyrocatechol-on-anatase TiO_2 (101) system, based on our findings. The positions of the occupied states in anatase TiO_2 and pyrocatechol adsorbed on anatase TiO_2 are taken from the corresponding valence band spectra. The position of the HOMO of unbound pyrocatechol is taken from the valence band of a thick film of pyrocatechol adsorbed on a TiO_2 substrate[17] and the separation between the HOMO and LUMO is set to be 4.5 eV, as determined from optical absorption measurements[61]. The position of the LUMO+1,2 states are taken from the Gaussian '03 simulations of the ground state energies of the pyrocatechol-on-anatase cluster, plotted relative to the LUMO + 7 (which is taken to be at the same energy as the LUMO of the unbound molecule). The HOMO to LUMO+7 separation in the cluster is assumed to be the same as the HOMO-LUMO separation of the molecule in solution (the calculations for the free molecule and the cluster support this). The LUMO+1,2 are the lowest-lying empty states of the pyrocatechol-on-anatase cluster that have some carbon character. They have very similar energies, both lying only 0.1 eV higher in energy than the LUMO. The separation between the HOMO and LUMO+1,2 is 3.9 eV. In order to estimate the onset of absorption for the transition between these states, in figure 7 we include Gaussians of 0.5 eV full width at half maximum, centred on the HOMO and LUMO+1,2 energies. This replicates the width of the π - π^* transition in unbound pyrocatechol in a typical optical absorption experiment[61]. This gives an onset of absorption of around 2.9 eV which is in good agreement with the 3 eV observed experimentally from UV-vis absorption measurements[27]. We expect this transition to have significant oscillator strength arising from the C π character of the LUMO+1,2, but both orbitals are nevertheless located mainly in the TiO_2 surface. The position of these states, very close in energy to the LUMO and near the bottom of the bulk TiO_2 conduction band can facilitate direct charge transfer from pyrocatechol into anatase TiO_2.

4. Conclusions

NEXAFS analysis of pyrocatechol adsorbed on anatase TiO_2 (101) and rutile TiO_2 (110) reveals the plane of the aromatic ring (defined by the σ* orbitals) to be similarly oriented on both surfaces at 27°±6° and 23°±8° respectively from the surface normal. The NEXAFS spectrum of pyrocatechol adsorbed on anatase shows additional features at approximately 283 eV, at lower photon energy than the main π* resonance.

Molecular orbital calculations of pyrocatechol adsorbed on an anatase TiO_2 (101) cluster indicate the appearance of new unoccupied states at lower energy than the LUMO of the isolated molecule due to states formed by bonding between the molecule and the surface. The calculations show that the LUMO of pyrocatechol adsorbed on an anatase cluster is located primarily on the TiO_2 surface, but the LUMO+1, LUMO+2 and LUMO+4 have some pyrocatechol C π* character. The LUMO+7 is similar to the LUMO of the isolated molecule. A NEXAFS simulation of the molecule adsorbed on the anatase cluster shows good agreement with the experimental spectrum of pyrocatechol adsorbed on anatase TiO_2 (101) supporting a bidentate adsorption geometry. It also replicates the low energy feature observed in the NEXAFS spectrum at ~283 eV, which is consistent with some C π* character in the new unoccupied states. We assign the feature at ~283 eV to the $C_{3\text{-}6} \rightarrow$ LUMO+1 and $C_{1,2} \rightarrow$ LUMO+2 transitions; both final states are selectively stabilized by the core-hole effect. While the LUMO+1, LUMO+2 and LUMO+4 orbitals have some C π* character, they are predominantly located in the TiO_2 surface, with energies above the conduction band of bulk TiO_2, but significantly below the LUMO of the unbound pyrocatechol molecule. The atomic character and energies of these unoccupied states of the adsorbate/surface complex can facilitate direct photoinjection from pyrocatechol to the TiO_2 surface as predicted by Persson *et al*.[27]. This adsorbate-induced modification of the surface electronic structure

allows us to rationalize the onset energy of the optical absorption of the pyrocatechol/anatase system. Our results emphasise the importance of the bonding at the adsorbate/surface interface in modifying the light-harvesting capabilities of dye-sensitised oxides in photovoltaics.

ACKNOWLEDGMENTS

The experimental work at Elettra and at MAX-lab was funded under The European Community's Seventh Framework Programme (FP7/2007-2013) under grant agreement no. 226716 and by EPSRC travel grant EP/H0020446/1. The authors thank Lars Petterson for help with StoBe-deMon calculations and Petter Persson for supplying coordinates for his original anatase TiO_2 (101) surface cluster calculation which was modified for this work.

SUPPORTING INFORMATION

Electron density distribution isosurfaces for the LUMO – LUMO+10 of the pyrocatechol molecule adsorbed on an anatase TiO_2 (101) cluster, obtained using Gaussian '03. This material is available free of charge via the Internet at http://pubs.acs.org

FIGURES

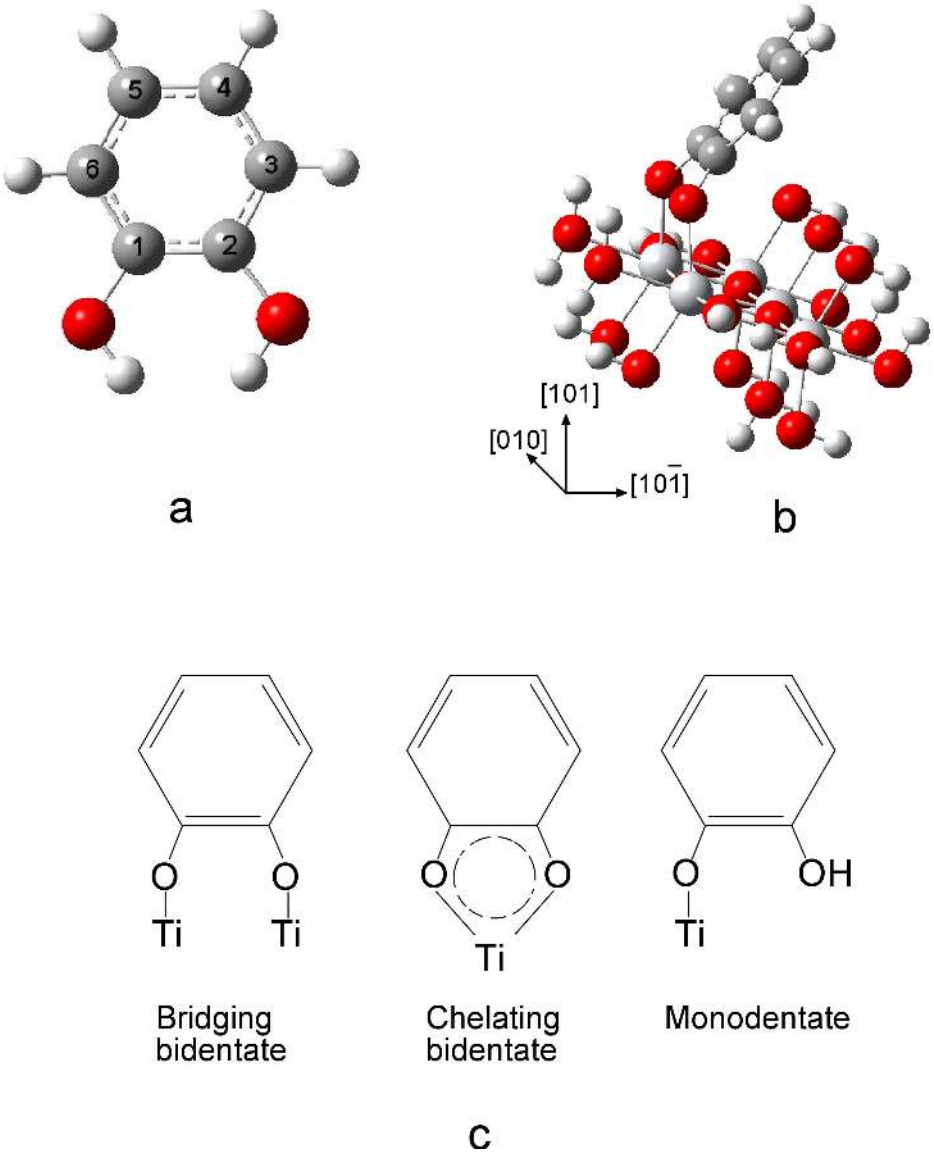

Figure 1 (a). Pyrocatechol molecule (geometry optimised). Grey spheres are carbon atoms, red spheres are oxygen atoms and white spheres are hydrogen atoms. The carbon atoms are numbered 1-6 for reference. (b) A pyrocatechol molecule adsorbed on an anatase TiO_2 (101) cluster (geometry optimized using Gaussian '03). Pale grey spheres are titanium atoms. (c) Schematic picture of the three possible structures catechol may adopt on a TiO_2 surface.

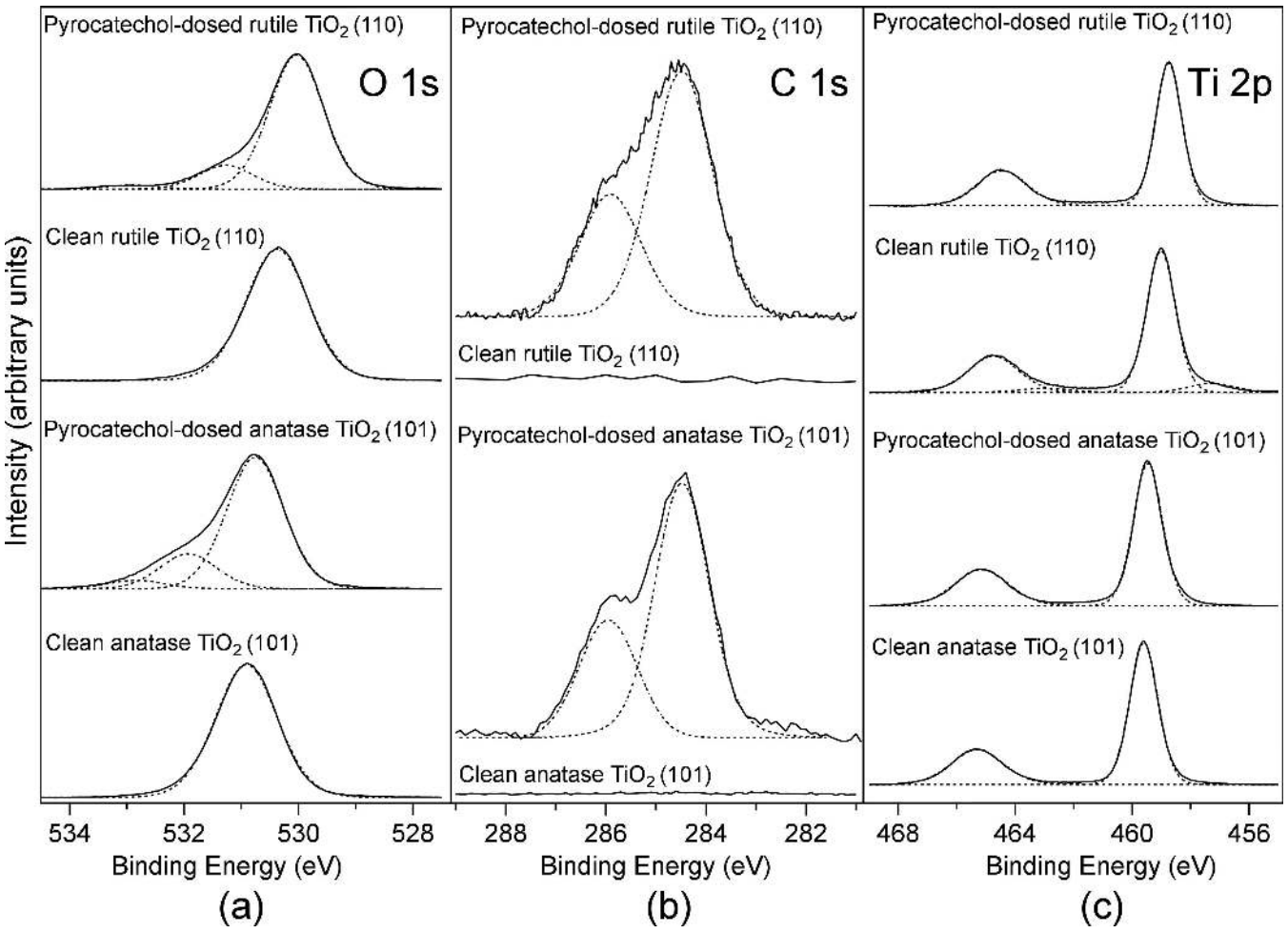

Figure 2. (a) O 1s spectra recorded at a photon energy of 700 eV for clean anatase TiO_2 (101), 1 ML pyrocatechol adsorbed on anatase TiO_2 (101), clean rutile TiO_2 (110) and 1 ML pyrocatechol adsorbed on rutile TiO_2 (110). (b) C 1s spectra recorded at a photon energy of 1000 eV for clean anatase TiO_2 (101), 1 ML pyrocatechol adsorbed on anatase TiO_2 (101), clean rutile TiO_2 (110) and 1 ML pyrocatechol adsorbed on rutile TiO_2 (110). (c) Ti 2p spectra recorded at a photon energy of 700 eV for clean anatase TiO_2 (101), 1 ML pyrocatechol adsorbed on anatase TiO_2 (101), clean rutile TiO_2 (110) and 1 ML pyrocatechol adsorbed on rutile TiO_2 (110). The dotted lines show Voigt curves (70% Gaussian:30% Lorentzian) fitted to the separate components (see text).

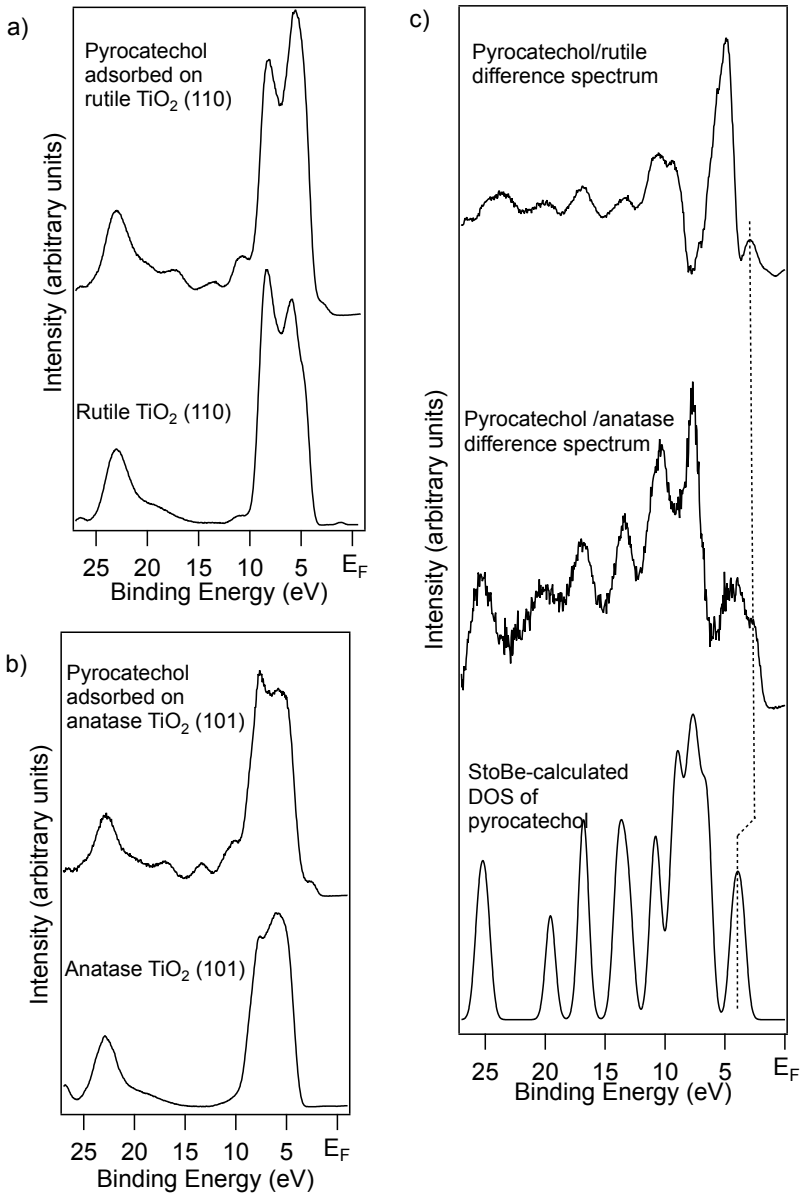

Figure 3. Valence band spectra recorded at a photon energy of 130 eV for (a) clean anatase TiO_2 (101) and 1 ML pyrocatechol adsorbed on anatase TiO_2 (101), (b) clean rutile TiO_2 (110) and 1 ML pyrocatechol adsorbed on rutile TiO_2 (110). (c) Valence band difference spectra (dosed-clean) for 1 ML pyrocatechol adsorbed on anatase TiO_2 (101) and rutile TiO_2 (110) compared to the StoBe-calculated density of states spectrum of pyrocatechol. The band-bending shift between the clean and pyrocatechol-dosed valence bands was accounted for before taking the difference spectrum. The dotted line shows the shift in energy between the experimental and calculated HOMOs (see text).

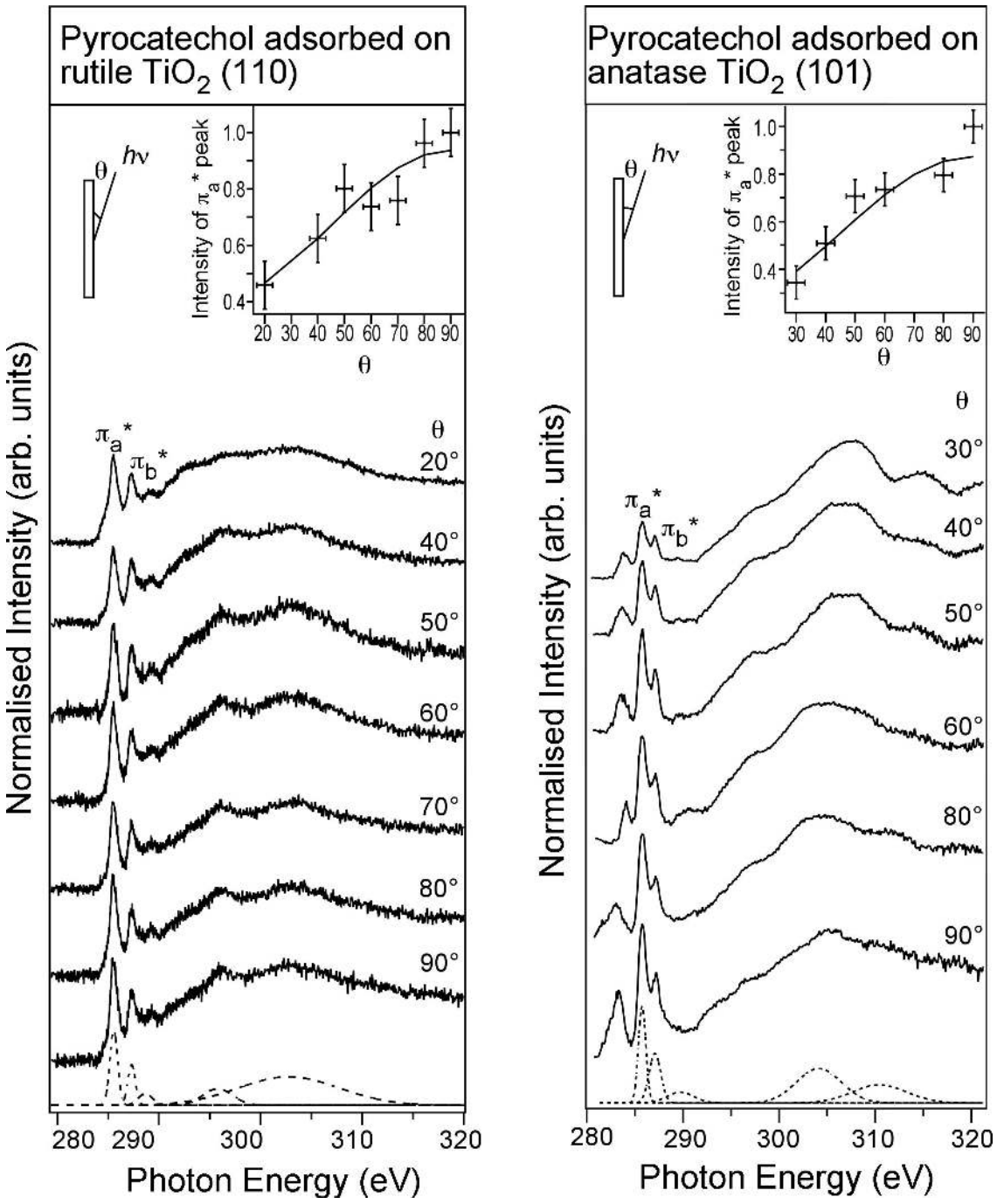

Figure 4. Carbon K edge NEXAFS spectra of 1 ML pyrocatechol adsorbed on rutile TiO_2 (110) and anatase TiO_2 (101) surfaces. The dotted lines show the Gaussians that give the best fit to the experimental data for the normal incidence spectra. The insets show the resulting areas of the π_a* peaks plotted as a function of angle of photon incidence to the surface and the Stöhr equations[56] fitted to the data points.

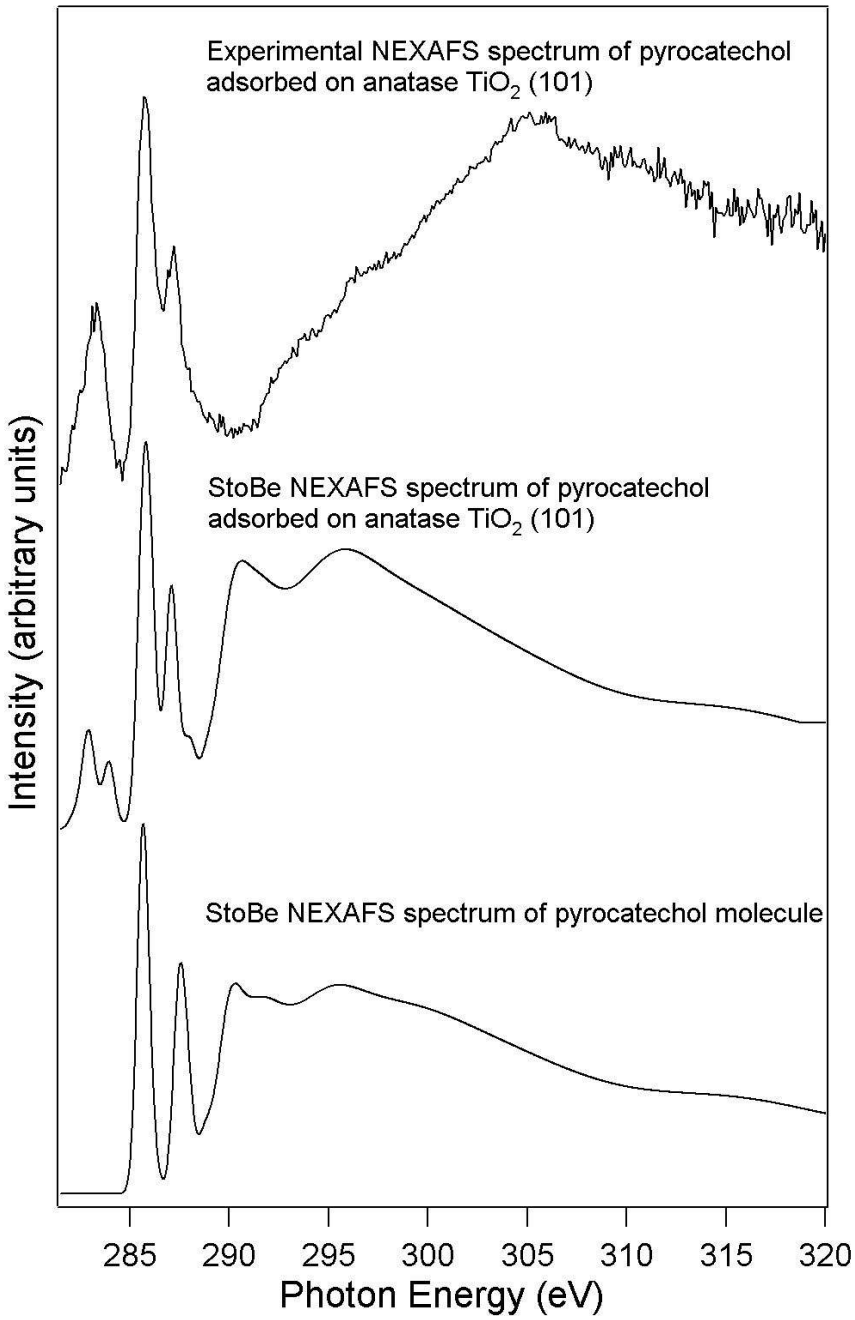

Figure 5. Comparison between the experimental carbon K-edge NEXAFS spectrum of 1 ML pyrocatechol adsorbed on anatase TiO_2 (101) (recorded at normal incidence), with the StoBe-generated carbon K-edge NEXAFS spectrum of pyrocatechol and pyrocatechol adsorbed on an anatase TiO_2 (101) cluster.

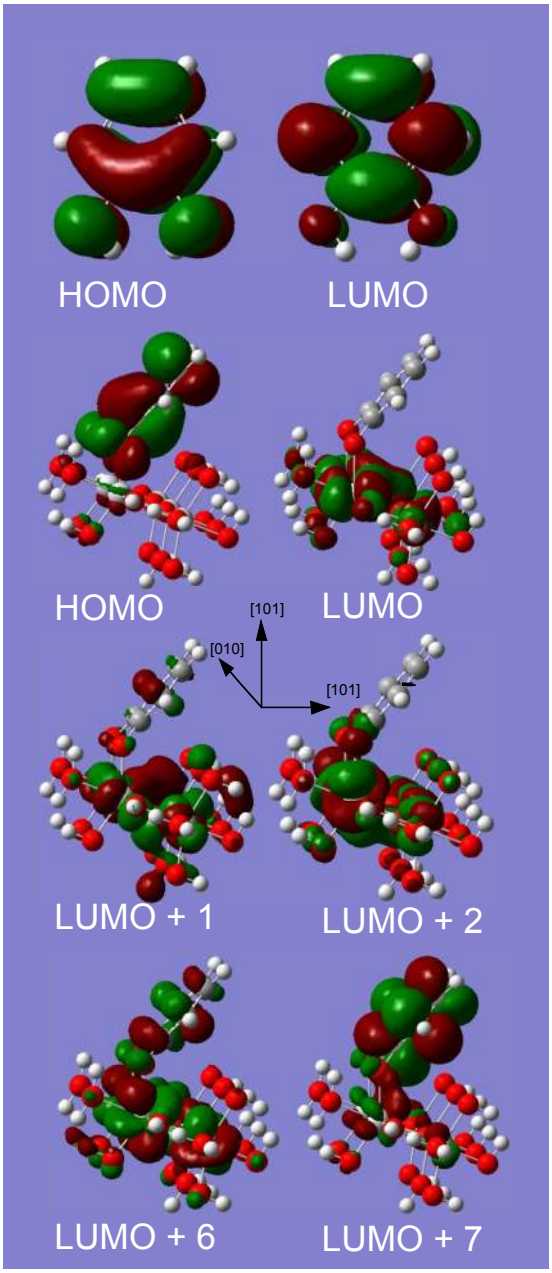

Figure 6. Electron density distribution isosurfaces for the HOMO and LUMO of the isolated pyrocatechol molecule (upper panel) and the pyrocatechol molecule adsorbed on an anatase TiO_2 (101) cluster (remaining panels), obtained using Gaussian '03. Also shown are the isosurfaces for the LUMO+1, LUMO+2, LUMO+6 and LUMO+7 of the pyrocatechol molecule adsorbed on an anatase TiO_2 (101) cluster.

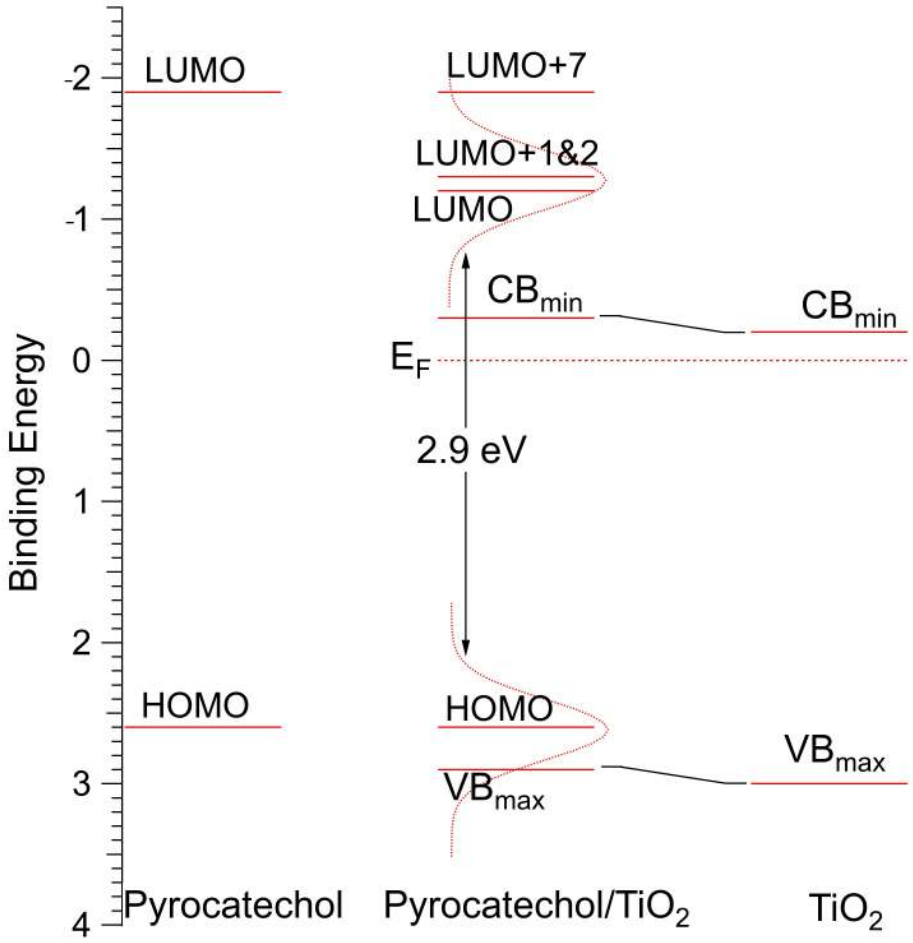

Figure 7. Schematic energy level diagram for pyrocatechol adsorbed on the anatase TiO_2 (101) surface, obtained using the method given in the text.

TABLES.

Table 1. O 1s peak assignments.

Binding Energy (eV) ±0.1 eV				
Clean anatase	Pyrocatechol adsorbed on anatase	Clean rutile	Pyrocatechol adsorbed on rutile	**Assignment**
530.9 (100 %)	530.8 (74.9±0.7 %)	530.4 (100 %)	530.0 (82.7±0.4 %)	oxygen atoms in TiO_2 surface[38]
	531.9 (19.8±2.3 %)		531.3 (14.7±2.0 %)	oxygen atoms in pyrocatechol[39]
	532.8 (5.2±2.7%)		532.9 (2.5±2.3 %)	hydroxyl groups[39]

Binding energies, relative abundances as a percentage of total O 1s signal (in brackets) and assignment of peaks fitted to the O 1s spectra of the clean TiO_2 surfaces and 1 ML pyrocatechol adsorbed on anatase TiO_2 (101) and rutile TiO_2 (110).

Table 2. C 1s peak assignments.

Binding Energy (eV) ±0.1 eV		
Pyrocatechol adsorbed on anatase	Pyrocatechol adsorbed on rutile	**Assignment**
284.6 (66.3±2.8 %)	284.5 (66.7±5.3 %)	carbon atoms 3-6 in figure 1[42]
286.1 (33.7±5.2 %)	285.9 (33.3±9.5 %)	carbon atoms 1-2 in figure 1[42]

Binding energies, relative abundances as a percentage of total C 1s signal (in brackets) and assignment of peaks fitted to the C 1s spectra of 1 ML pyrocatechol adsorbed on anatase TiO_2 (101) and rutile TiO_2 (110).

Table 3. Ti 2p peak assignments.

Binding Energy (eV) ±0.1 eV				
Clean anatase	Pyrocatechol adsorbed on anatase	Clean rutile	Pyrocatechol adsorbed on rutile	**Assignment**
		457.3 (6.3±2.9 %)		Ti^{3+}: $2p_{3/2}$ [45]
459.6 (68.9±1.3 %)	459.5 (67.9±1.9 %)	459.0 (62.7±1.2 %)	458.8 (68.9±1.2 %)	Ti^{4+}: $2p_{3/2}$ [44]
		463.0 (3.1±2.9 %)		Ti^{3+}: $2p_{1/2}$ [45]
465.3 (31.1±2.8%)	465.1 (32.1±3.7 %)	464.8 (27.9±2.2 %)	464.5 (31.1±2.5 %)	Ti^{4+}: $2p_{1/2}$ [44]

Binding energies, relative abundances as a percentage of total Ti 2p signal (in brackets) and assignment of peaks fitted to the Ti 2p spectra of the clean TiO_2 surfaces and 1 ML pyrocatechol adsorbed on anatase TiO_2 (101) and rutile TiO_2 (110).

REFERENCES

(1) Chen, Z. Y.; Hu, Y.; Liu, T. C.; Huang, C. L.; Jeng, T. S. *Thin Solid Films* **2009**, *517*, 4998.

(2) O' Regan, B.; Grätzel, M. *Nature* **1991**, *353*, 737.

(3) Tengvall, P.; Lundstrom, I. *Clinical Materials* **1992**, *9*, 115.

(4) Paz, Y.; Luo, Z.; Rabenberg, L.; Heller, A. *J. Mater. Res.* **1995**, *10*, 2842.

(5) Chen, W. J.; Tsai, P. J.; Chen, Y. C. *Small* **2008**, *4*, 485.

(6) Lee, H.; Scherer, N. F.; Messersmith, P. B. *Proceedings of the National Academy of Sciences of the United States of America* **2006**, *103*, 12999.

(7) Liu, J. Q.; de la Garza, L.; Zhang, L. G.; Dimitrijevic, N. M.; Zuo, X. B.; Tiede, D. M.; Rajh, T. *Chemical Physics* **2007**, *339*, 154.

(8) Thomas, A.; Syres, K. *Chem. Soc. Rev.* **2012**, *41*, 4207.

(9) Nazeeruddin, M. K.; Kay, A.; Rodicio, I.; Humphrybaker, R.; Muller, E.; Liska, P.; Vlachopoulos, N.; Gratzel, M. *Journal of the American Chemical Society* **1993**, *115*, 6382.

(10) Fillinger, A.; Soltz, D.; Parkinson, B. A. *J. Electrochem. Soc.* **2002**, *149*, A1146.

(11) Gong, X. Q.; Selloni, A.; Batzill, M.; Diebold, U. *Nature Materials* **2006**, *5*, 665.

(12) He, Y. B.; Dulub, O.; Cheng, H. Z.; Selloni, A.; Diebold, U. *Physical Review Letters* **2009**, *102*, 4.

(13) Li, S. C.; Losovyj, Y.; Diebold, U. *Langmuir* **2011**, *27*, 8600.

(14) Liu, L. M.; Li, S. C.; Cheng, H. Z.; Diebold, U.; Selloni, A. *Journal of the American Chemical Society* **2011**, *133*, 7816.
(15) Hengerer, R.; Bolliger, B.; Erbudak, M.; Grätzel, M. *Surface Science* **2000**, *460*, 162.
(16) Hengerer, R.; Kavan, L.; Krtil, P.; Gratzel, M. *J. Electrochem. Soc.* **2000**, *147*, 1467.
(17) Syres, K.; Thomas, A.; Bondino, F.; Malvestuto, M.; Grätzel, M. *Langmuir* **2010**, *26*, 14548.
(18) Thomas, A.; Syres, K. *Applied Physics Letters* **2012**, *100*, 171603.
(19) Thomas, A. G.; Flavell, W. R.; Chatwin, C.; Rayner, S.; Tsoutsou, D.; Kumarasinghe, A. R.; Brete, D.; Johal, T. K.; Patel, S.; Purton, J. *Surface Science* **2005**, *592*, 159.
(20) Thomas, A. G.; Flavell, W. R.; Kumarasinghe, A. R.; Mallick, A. K.; Tsoutsou, D.; Smith, G. C.; Stockbauer, R.; Patel, S.; Grätzel, M.; Hengerer, R. *Physical Review B* **2003**, *67*, 035110.
(21) Lotnyk, A.; Senz, S.; Hesse, D. *Thin Solid Films* **2007**, *515*, 3439.
(22) Ong, C. K.; Wang, S. J. *Applied Surface Science* **2001**, *185*, 47.
(23) Herman, G. S.; Gao, Y. *Thin Solid Films* **2001**, *397*, 157.
(24) Diebold, U. *Surf. Sci. Rep.* **2003**, *48*, 53.
(25) Bikondoa, O.; Pang, C. L.; Ithnin, R.; Muryn, C. A.; Onishi, H.; Thornton, G. *Nature Materials* **2006**, *5*, 189.
(26) Duncan, W. R.; Prezhdo, O. V. *Annu. Rev. Phys. Chem.* **2007**, *58*, 143.
(27) Persson, P.; Bergstrom, R.; Lunell, S. *Journal of Physical Chemistry B* **2000**, *104*, 10348.
(28) Creutz, C.; Chou, M. H. *Inorg. Chem.* **2008**, *47*, 3509.
(29) Schnadt, J.; Bruhwiler, P. A.; Patthey, L.; O'Shea, J. N.; Sodergren, S.; Odelius, M.; Ahuja, R.; Karis, O.; Bassler, M.; Persson, P.; Siegbahn, H.; Lunell, S.; Martensson, N. *Nature* **2002**, *418*, 620.
(30) Duncan, W. R.; Prezhdo, O. V. *Journal of Physical Chemistry B* **2005**, *109*, 365.
(31) Gundlach, L.; Ernstorfer, R.; Willig, F. *Physical Review B* **2006**, *74*.
(32) Redfern, P. C.; Zapol, P.; Curtiss, L. A.; Rajh, T.; Thurnauer, M. C. *Journal of Physical Chemistry B* **2003**, *107*, 11419.
(33) Rodriguez, R.; Blesa, M. A.; Regazzoni, A. E. *Journal of Colloid and Interface Science* **1996**, *177*, 122.
(34) Li, S. C.; Wang, J. G.; Jacobson, P.; Gong, X. Q.; Selloni, A.; Diebold, U. *Journal of the American Chemical Society* **2009**, *131*, 980.
(35) Thomas, A. G.; Flavell, W. R.; Kumarasinghe, A. R.; Mallick, A. K.; Tsoutsou, D.; Smith, G. C.; Stockbauer, R.; Patel, S.; Grätzel, M.; Hengerer, R. *Phys. Rev. B* **2003**, *67*.
(36) Frisch, M. J.; Trucks, G. W.; Schlegel, H. B.; Scuseria, G. E.; Robb, M. A.; Cheeseman, J. R.; Montgomery, J. A.; Vreven, T.; Kudin, K. N.; Burant, J. C.; et al. Gaussian 03 Revision B.04; Gaussian, Inc.: Wallingford CT, 2004.
(37) Hermann, K.; Pettersson, L. StoBe-deMon SOFTWARE, Stockholm-Berlin version 2.2 of deMon, 2006.
(38) Ben Taylor, J.; Mayor, L. C.; Swarbrick, J. C.; O'Shea, J. N.; Schnadt, J. *J. Phys. Chem. C* **2007**, *111*, 16646.
(39) Mayor, L. C.; Ben Taylor, J.; Magnano, G.; Rienzo, A.; Satterley, C. J.; O'Shea, J. N.; Schnadt, J. *Journal of Chemical Physics* **2008**, *129*.
(40) Patthey, L.; Rensmo, H.; Persson, P.; Westermark, K.; Vayssieres, L.; Stashans, A.; Petersson, A.; Bruhwiler, P. A.; Siegbahn, H.; Lunell, S.; et al. *Journal of Chemical Physics* **1999**, *110*, 5913.
(41) Johansson, E. M. J.; Plogmaker, S.; Walle, L. E.; Scholin, R.; Borg, A.; Sandell, A.; Rensmo, H. *J. Phys. Chem. C* **2010**, *114*, 15015.
(42) Weinhold, M.; Soubatch, S.; Temirov, R.; Rohlfing, M.; Jastorff, B.; Tautz, F. S.; Doose, C. *Journal of Physical Chemistry B* **2006**, *110*, 23756.
(43) Jacobson, P.; Li, S. C.; Wang, C.; Diebold, U. *J. Vac. Sci. Technol. B* **2008**, *26*, 2236.

(44) Armitage, D. A.; Grant, D. M. *Mater. Sci. Eng. A-Struct. Mater. Prop. Microstruct. Process*. **2003**, *349*, 89.

(45) Bertoti, I.; Mohai, M.; Sullivan, J. L.; Saied, S. O. *Applied Surface Science* **1995**, *84*, 357.

(46) Yim, C. M.; Pang, C. L.; Thornton, G. *Physical Review Letters* **2010**, *104*.

(47) Wang, L. Q.; Shultz, A. N.; Baer, D. R.; Engelhard, M. H. *Journal of Vacuum Science & Technology a-Vacuum Surfaces and Films* **1996**, *14*, 1532.

(48) Thomas, A. G.; Flavell, W. R.; Mallick, A. K.; Kumarasinghe, A. R.; Tsoutsou, D.; Khan, N.; Chatwin, C.; Rayner, S.; Smith, G. C.; Stockbauer, R. L. et al. *Phys. Rev. B* **2007**, *75*.

(49) Henrich, V. E.; Cox, P. A. *The Surface Science of Metal Oxides*; Cambridge University Press: Cambridge, 1994.

(50) Thompson, T. L.; Yates, J. T. *Chemical Reviews* **2006**, *106*, 4428.

(51) Ganduglia-Pirovano, M. V.; Hofmann, A.; Sauer, J. *Surf. Sci. Rep*. **2007**, *62*, 219.

(52) Wendt, S.; Sprunger, P. T.; Lira, E.; Madsen, G. K. H.; Li, Z. S.; Hansen, J. O.; Matthiesen, J.; Blekinge-Rasmussen, A.; Laegsgaard, E.; Hammer, B.; Besenbacher, F. *Science* **2008**, *320*, 1755.

(53) Flavell, W. R.; Laverty, J. H.; Law, D. S. L.; Lindsay, R.; Muryn, C. A.; Flipse, C. F. J.; Raiker, G. N.; Wincott, P. L.; Thornton, G. *Physical Review B* **1990**, *41*, 11623.

(54) Carbone, M.; Piancastelli, M. N.; Casaletto, M. P.; Zanoni, R.; Besnard-Ramage, M. J.; Comtet, G.; Dujardin, G.; Hellner, L. *Surface Science* **1999**, *419*, 114.

(55) Solomon, J. L.; Madix, R. J.; Stohr, J. *Surface Science* **1991**, *255*, 12.

(56) Stöhr, J. *NEXAFS Spectroscopy*; Springer-Verlag: Berlin, 2003.

(57) Thomas, A. G.; Flavell, W. R.; Chatwin, C. P.; Kumarasinghe, A. R.; Rayner, S. M.; Kirkham, P. F.; Tsoutsou, D.; Johal, T. K.; Patel, S. *Surface Science* **2007**, *601*, 3828.

(58) De Angelis, F.; Fantacci, S.; Selloni, A.; Gratzel, M.; Nazeeruddin, M. K. *Nano Letters* **2007**, *7*, 3189.

(59) Oji, H.; Mitsumoto, R.; Ito, E.; Ishii, H.; Ouchi, Y.; Seki, K.; Yokoyama, T.; Ohta, T.; Kosugi, N. *Journal of Chemical Physics* **1998**, *109*, 10409.

(60) Plashkevych, O.; Yang, L.; Vahtras, O.; √Ögren, H.; Petterson, L. G. M. *Chemical Physics* **1997**, *222*, 125.

(61) Liu, Y.; Dadap, J. I.; Zimdars, D.; Eisenthal, K. B. *The Journal of Physical Chemistry B* **1999**, *103*, 2480.